Femtomolar detection of Cu2+ ions in solution using super-Nernstian FET-sensor with a lipid monolayer as top-gate dielectric

A. Kenaan, F. Brunel, J.-M. Raimundo, Anne Charrier

Sensors & actuators B: Chemistry, 316, 128147 (2020)

DOI: 10.1016/j.snb.2020.128147

Femtomolar detection of Cu^{2+} ions in solution using super-Nernstian FET-sensor with a lipid monolayer as top-gate dielectric

A. Kenaan[a,§], F. Brunel[a], J.-M. Raimundo[a,*], A.M. Charrier[a,*]

[a] *Aix Marseille Univ, CNRS, CINAM, Marseille, France*

ABSTRACT: The development of ions sensors with low limit of detection and high sensitivity and selectivity is required in many fields of application and still remains a challenge. We report on the first dual-gated field effect transistor sensor with an engineered lipid monolayer as top gate dielectric. The sensor was designed and fabricated for the specific detection of Cu^{2+} using the Di-2-picolylamine as recognition unit. The lipid monolayer was reticulated to achieve high mechanical and dielectric stability over device operation. The resulting sensor exhibits exceptional performances with a limit of detection at 10 femtomolar, with a linear dependency over 10 decades and a super-Nernstian sensitivity of ~100 mV/decade. We also show that the lipid layer forms a good barrier to ions trapping, hence providing a high stability of the sensor over measurements.

* Corresponding authors.
E-mail addresses: ahmed.kenaan@york.ac.uk (A. Kenaan), brunel@cinam.univ-mrs.fr (F. Brunel), jean-manuel.raimundo@univ-amu.fr (J.-M. Raimundo), anne.charrier@univ-amu.fr (A.M. Charrier)

§ Present address: University of York, Department of physics, York, UK

Keywords: Electrolyte dual-gated field effect transistor; lipid monolayer; Cu^{2+} detection; di-picolylamine-based chelator; ultra-thin dielectric

1. Introduction

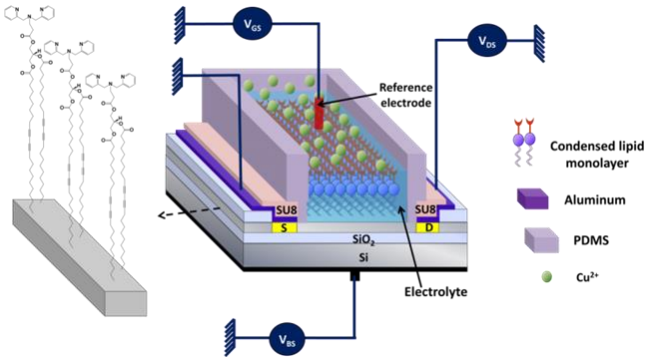

Fig. 1. Schematic illustration of the FET sensor.

Ion sensors are required in many domains of the society including environment (Cinti et al., 2018; Brezoczki et al., 2017; Strungaru et al., 2018), technology (Arbadi et al., 2016) and security (Zhang et al., 2018) with the highest societal impact in the biomedical field (Kubala-Kukuś et al., 2014; Wustoni et al., 2015). The detection of low concentration molecules/ions of biological or physiological interest in the body with high sensitivity and selectivity is an ultimate goal that offers new opportunities in the early diagnostic and treatment of diseases. Among the ions of interest, copper (II) is an essential nutrient ensuring proper organs function such as in brain, heart, and the development of bones or connective tissues. However, its body accumulation due to excess intake or genetic condition can lead to dramatic tissue injury (Filetti et al., 2018) or diseases such as the Wilson's disease (Das et al., 2006; Roberts et al., 2008). Although an early diagnosis allows the efficient and complete treatment of the illness, failure to diagnose a Wilson's disease patient can result in irreversible clinical damages and death. From environmental and industrial perspective, it is crucial to monitor the concentrations of Cu^{2+} in industrial effluents; Cu^{2+} is indeed phytotoxic, and an excess in freshwater resources and aquatic ecosystem damages the osmo-regulatory mechanism of the freshwater animals (Brezoczki et al., 2017; Arbadi et al, 2016).

These examples illustrate the need for appropriate sensors for Cu^{2+} detection in solution. Whereas spectroscopic techniques such as inductive coupled plasma mass spectroscopy (ICP-MS) (Kilic et al., 2018; Quinn et al., 2018) or atomic absorption spectroscopy (AAS) (Ghisi et al., 2011) are the most commonly used and the most sensitive ones (limit of detection (LOD) down to the picomolar range) for the detection of ions in solution, they

usually require expensive and large equipment. They also often require pre-concentration and/or filtering of the analytes, which all together prevent on-site, real time detection or systematic analysis. Recently more suitable devices for low cost and on-site measurements have been developed based on both colorimetric (Gao et al., 2017) and fluorescence (Zhang et al., 2018; Liu et al., 2018) optical spectroscopies, electrochemical (Cinti et al., 2018) or photo-electrochemical (Wang et al., 2018) techniques combined with a metal-ligand to increase selectivity. However, most of these devices are limited in term of LOD to the nanomolar or picomolar range. Ion sensitive Field effect transistor (ISFET) sensors constitute another class of sensors that are highly suitable for the detection of ions in solution due to the high sensitivity of FET response to electrical charges. In such devices the selectivity is usually ensured by grafting a specific probe to the gate dielectric (Wang et al., 2018). For Cu^{2+} FET sensors, prion protein (Wustoni et al., 2015), nitrilotriacetic acid (NTA) (Ma et al., 2018; Sasaki et al., 2017), Gly-Gly-His peptide (Nguyen et al., 2019) and thiacalix[4]arene (Takagiri et al., 2020) were used as metal ion ligand and demonstrated high selectivity. The LODs remained however higher than the picomolar level. Only recently a limit of detection of 10 fM was reported using a Si-nanoribbon FET (Synhaivska et al., 2019). In another work, FET composed of an engineered lipid monolayer as ultra-thin gate dielectric was demonstrated to provide very low limit of detection down to 50 fM with a good selectivity towards Fe^{3+} ions (Nguyen et al., 2014). These advanced self-assembled lipid monolayers, obtained by reticulation of the lipids, present exceptional dielectric strength in the range 20 to 30 MV/cm (Dumas et al., 2011; Kenaan et al., 2018) and good mechanical stability (Charrier et al., 2010; El Zein et al., 2012). Additionally, these layers are extremely versatile and can be easily chemically customized to impart specific functionalities (Kenaan et al., 2018; Nguyen et al., 2013). Such layers were also used for the fabrication of micro-array as capacitive sensing platforms to detect and quantify ferric ions concentrations in solution (Kenaan et al., 2016). In both these studies the very low LOD is ascribed to the high capacity and exceptional insulating properties of the ultra-thin insulating layer and confirms the interest of such lipid-FET for the detection of low concentration small ions in solution.

In this work we present the first dual-gated ISFET sensor based on a chemically engineered lipid monolayer as both top-gate dielectric and sensitive layer developed for the detection of Cu^{2+} ions, whereas the back-gate dielectric is made of silicon dioxide. In contrast to previously reported dual-gated ISFET always working in enhancement mode, our novel sensor works in depletion mode. The selectivity is ensured by a di-(2-picolyl)amine (Dpa)

derivative as probe which is grafted to the lipids after modification of their head-group. Dpa is a well-studied chelator which presents high selectivity for Cu^{2+} ions (Hoorn et al., 1996; Cho et al., 2019; Dugandžić et al. 2019). The synthesis of the modified lipids and the fabrication of the lipid monolayer are detailed hereby. Detection measurements for Cu^{2+} in aqueous medium are reported and the performances of such sensor are outstanding with a LOD of 10 fM and a super-Nernstian sensitivity of ~100 mV/decade.

2. Materials and methods

2.1. Physicochemical Analysis of chelator end-capped lipids

^{1}H and ^{13}C NMR spectra were recorded on a Bruker AC 250 at 250 and 62.5 MHz, respectively. Mass measurements were performed on an Ultraflex II MALDI-TOF/TOF mass spectrometer (Bruker Daltonics, Bremen, Germany) equipped with a Smartbeam laser (355 nm, 200 Hz) in the positive reflector mode. Lipid sample (in 100% chloroform) was mixed with the matrix solution, a saturated solution of 2,5-Dihydroxybenzoic acid (DHB, Sigma Aldrich) in 30% acetonitrile and 0.1% trifluoroacetic acid, in a 1:1 ratio (v/v) and the mixture (1 µL) was deposited on a polished steel MALDI target plate.

2.2. Physicochemical Measurements in Solution.

UV–visible absorption spectra were obtained on a Varian Cary 1E spectrophotometer. The absorption maxima (λ_{max}) are directly extracted from absorption spectra of chelator **3** based solution. Under the optimum conditions, the stoichiometry between chelator **3** and Cu^{2+} was investigated by the molar ratio method (Job, 1971) in UV–visible. Affinity constants were extracted from ^{1}H NMR titration experiments performed at 25 °C using a JEOL ECS-400 spectrometer operating at 400 MHz. Before the experiment Dpa-lipid was dissolved in a 1:1: mixture of chloroform-*d* and methanol-*d* (final concentration 1mM) in a NMR tube. Chelator/ion mixtures were obtained by successive addition ion dissolved in D_2O directly into the NMR tube (15 additions of 0.1 eq.). The affinity constant was then graphically determined using the Rose-Drago method (Rose and Drago, 1959; Wachter and Fried, 1974; Fielding, 2000).

2.3. Transistor fabrication

The transistors were fabricated from scratch at the PLANETE CT-PACA facility (CINaM, Marseille, France) starting from a SOI wafer with a silicon layer of 340 nm in thickness and a buried oxide of 1 µm. The transistors were fabricated using classical optical

photolithography (PL) in three steps that are described in the SI. To contain the solutions, a well made from polydimethylsiloxane (PDMS) was glued on top of the channel.

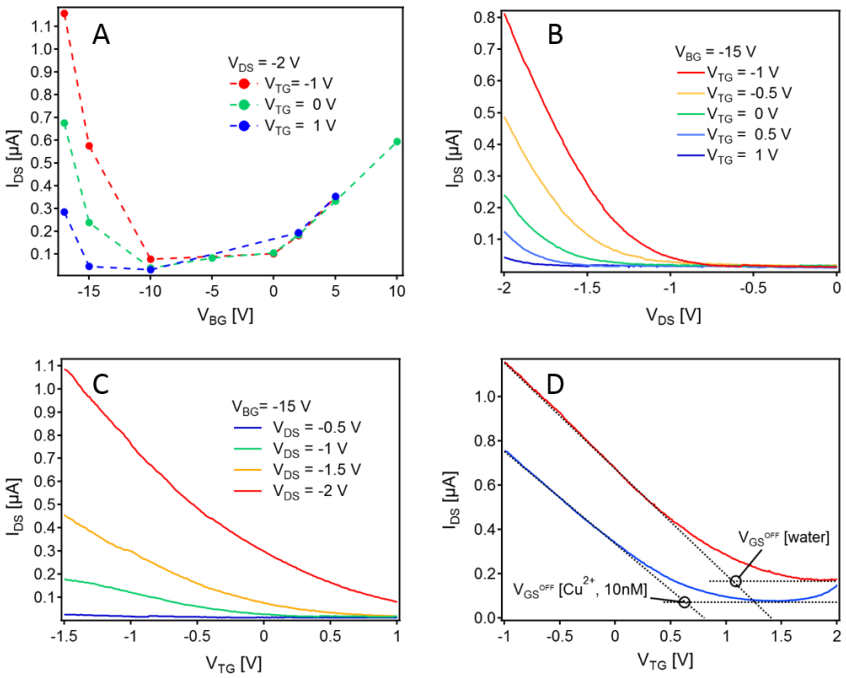

Fig. 2. (A) Effect of Back gate voltage (V_{bg}) on I_{DS} at different top gate voltage, V_{tg}; **(B)** Output and **(C)** transfer curves, respectively. **(D)** Transfer curves obtained in water (red) and after exposure of the sensor to 10 nM Cu^{2+} solution (blue) showing a shift of V_{GS}^{OFF} towards the negative values.

2.4. Lipid monolayer formation on transistor silicon channel

Lipid monolayer supported on H-terminated silicon transistor channel was formed using a protocol developed in the laboratory based on the vesicle fusion method (Charrier et al., 2005). Small unilamellar lipid vesicles were first obtained as follows: 100 µL of 0.1% lipid stock solution in chloroform was heated at 50°C until the chloroform was evaporated, then it was re-diluted in 100 µL of deionized water. Next, the lipid solution was sonicated for 30 min and extruded across 100 nm pores polycarbonate membranes. Just before lipid deposition, the native oxide of FET sensor was etched-off from silicon channel using 2% HF solution. The lipid solution was then poured onto the silicon channel at room temperature and then cooled down to 10°C. The temperature was then slowly increased to 32°C at 1°C/min. At this stage a DC-OH monolayer was formed. The crosslinking of the aliphatic chains was achieved by radical polymerization using 1% free radical AAPH initiator (2,2′-Azobis(2-methylpropionamidine) dihydrochloride) in water and subsequently increasing the temperature to 42°C. After 45 min. the sample was cooled down and rinsed with deionized water. At this stage the lipids form a homogeneous monolayer with a thickness of ~2.2 nm as confirmed by AFM imaging and measuring the

thickness by making a hole in the layer with the AFM tip. A scheme of the resulting device is depicted in Fig. 1.

2.5. Electrical Measurements

Static electrical transistor characteristics (output curves and transfer curves) were performed using a HP 4140B pico-ammeter/DC voltage source apparatus that provides both voltage sources and current readings for Top Gate-Source (V_{TG}) and Drain-Source (V_{DS}) polarizations. Another DC voltage source (TTI, PL330DP) was used to polarize the back-gate (V_{BG}). The top gate contact was an Ag/AgCl reference electrode dipped into the electrolyte solution.

2.6. Transistors operating conditions

The transistors used in this study consisted in a *p*-channel MOSFETs working in depletion mode, *i.e.* the transistor was normally "ON" at V_{TG}= 0 V. To obtain optimal transistor response, the working conditions were established as follows: a negative potential was applied to the drain, and the source was grounded. A negative potential was applied to the back gate offering good transistor response by varying the top-gate (Fig. 2A). High top-gate sensitivity was obtained for negative values of V_{BG} larger than -15 V as confirmed by the transfer and output curve measurements (Fig. 2B-C). To prevent lipid layer damages, V_{DS} was limited to [-2 V; 2 V] range and V_{TG} to [-1 V; 2 V] range. All transfer curves were performed at V_{DS}= -2 V. Under these conditions, the output curves do not reach the saturation, hence all measurements were performed in the triode regime. Under these experimental conditions, the capture of a positive charge by the probes at the top gate (lipid layer) surface induces a reduction of the current in the channel such as demonstrated in Fig. 2D.

2.7. Sensing measurements protocol

All sensing measurements were performed according to the following protocol: 1- a reference transfer curve is measured in di-ionized water (DI-water, ρ=18.2 MΩ.cm) by introducing 100 µl of water in the PDMS well. 2- the water is removed and replaced by 100 µl of a solution of $CuSO_4.5H_2O$ at a concentration of [X] M. The analyte solution is left over 10 min to allow copper complexation with the chelator. 3- the ion solution is carefully rinsed with DI-water to remove the ions in excess from the solution. Transfer curve is then acquired (Note that transfer curve is always obtained in DI water). 4- to remove the chelated ions a 10^{-3} M aqueous solution of NaOH was used. The well was then carefully

rinsed several times with DI water. The four steps were repeated successively for each concentration. Because the device response varies from one device to another, all the data reported here (except for the selectivity measurements) were obtained from three independent sets of measurement using the same device.

3. Results and discussion

3.1. Di-(2-picolyl) amine end-capped lipid probes (dpa-lipid)

The synthesis of the chelator functionalized lipid **3** is outlined in Scheme **1**. Molecule **3** was readily obtained from the cross-coupling reaction of the *N*-(3-Propionic acid) bis(2-pyridylmethyl) amine **1** with the cleaved DCPC **2** in 53% yield. **1** was prepared according to reported procedures (Bhattacharya et al; 2003, Pimentel et al, 2007; Wong et al., 2010) from 2-pyridinecarboxaldehyde in three steps affording the target compound in 97% overall yield. 10,12-tricosadiynoic acid -[1-(hydroxymethyl)-1,2-ethanediyl] ester **2** (DC-OH) lipids were obtained after cleavage of the commercially available DC8,9PC phosphocholine head-group by enzymatic reaction using phospholipase C according to Nguyen *et al*. procedure (Nguyen, 2014). Hereby is described the synthetic procedure to obtain the Dpa-lipid **3**. The bis(2-pyridylmethyl) amine core was selected due its well-known affinity to metallic species in particular for Cu^{2+} and can be tailored to adjust its complexation properties (Routasalo et al., 2008). In addition, bis(2-pyridylmethyl) amine is commercially available or can be readily synthetized at low cost rendering this chelator highly attractive associated with the possibilities to easily functionalize it.

At room temperature under an argon atmosphere, a solution of 0.1800 g (0.24 mmol, 1.0 equiv) of cleaved DCPC and 0.0740 g (0.29 mmol, 1.2 equiv) of 2-chloro-1-methylpyridinium iodide dissolved in 2 mL of dry dichloromethane (DCM) was added dropwise to a solution of 0.0650 g (0.24 mmol, 1 equiv) of Dpa carboxylic acid and 0.1070 g (0.58 mmol, 2.4 equiv) of tributylamine dissolved in 2 mL of dry DCM. later, the reaction mixture was refluxed for 3 hours. The solvent was then removed under reduced pressure and the residue was purified over a SiO_2 column chromatography using 5% of MeOH in DCM as eluent, yielding 0.1260 g (53%, 0.126 mmol) of the titled compound. ^{1}H NMR (400 MHz, $CDCl_3$, ppm): δ 8.51 (d, *J* = 5.2 Hz, 2H), 7.65 (t, *J* = 7.2 Hz, 2H), 7.45 (d, *J* = 8 Hz, 2H), 7.14 (t, *J* = 6.2 Hz, 2H), 5.19 (q, *J* = 4.8 Hz, 1H), 4.23 (m, 2H), 4.11 (m, 2H), 3.82 (s, 4H), 2.92 (t, *J* = 7.2 Hz, 2H), 2.58 (t, *J* = 7.2 Hz, 2H), 2.36-2.17 (br, 12H), 1.65-1.38 (br, 12H), 1.37-1.12 (br, 48H), 0.84 (t, *J* = 6.6 Hz, 6H) (Fig. S3). MS (MALDI-TOF) m/z: 1002.684 $[M + H]^+$; calculated for [M + H]+: 1002.730 $[M + H]^+$ (Fig. S2).

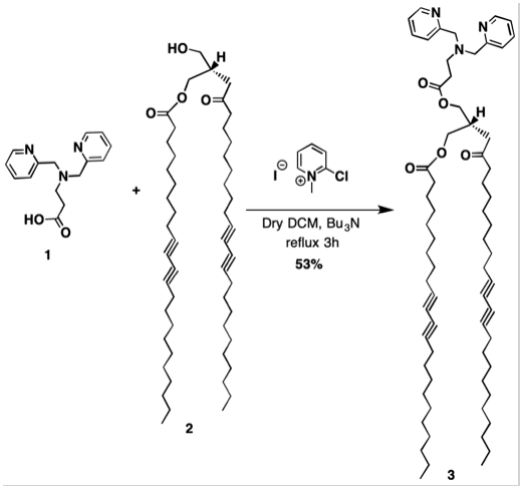

Scheme 1: Scheme **1**: Synthesis of **3**: 2-Chloro-1-methylpyridinium iodide, Bu_4N, dry DCM reflux 3h. (53%)

3.2. Complexation properties of Dpa end-capped lipid probes

The cation binding properties of the novel Dpa-lipid probe **3** was investigated by UV/Visible absorption spectroscopy using the Job's method of continuous variation (Fig. 3A-B). Compound **3** exhibits one main broad absorption band, centered at 257 nm, which displays several shoulders. Compound **3** interacts with putative cation guests emphasizing different degrees of spectroscopic changes depending on the nature of the cation, its charge and size. The binding of the cation with **3** results in a slight change of the absorption properties, requesting a gaussian fitting, associated with hyperchromic and hypochromic effects. The Job plots suggest the formation of a [1+1] complexes $\mathbf{3.X^{n+}}$ in agreement with results previously reported in literature on similar systems (Routasalo et al., 2008) (Fig.3B). For instance, S3 (ESI) displays the evolution of the absorption spectra obtained for 11 different fractions of Cu^{2+} and **3** (See Table S3 for solutions compositions, total product concentration 10^{-4} M) evidencing unambiguously a complexation of Cu^{2+} with **3** affording a $\mathbf{3.Cu^{2+}}$ complex. In addition, fine analysis of the data, fitted with 7 gaussians (Fig. 3A and S4), shows that upon the gradual addition of Cu^{2+}, the variations of the absorption properties of **3** are associated with hyperchromic effect for the peaks centered at 240 nm (P1), 250 nm (P2), and 257 nm (P3), hypochromic effect for the peaks at 262 nm (P5) and at 268 nm (P7) and hypsochromic effect with a small blue shift from 262 to 260 nm and from 268 to 266.5 nm. The peaks centered at 260 nm (P4) and 266.5 nm (P6) are mainly attributed to the formation of $\mathbf{3.Cu^{2+}}$complexes. From both UV-Vis and ^{1}H NMR

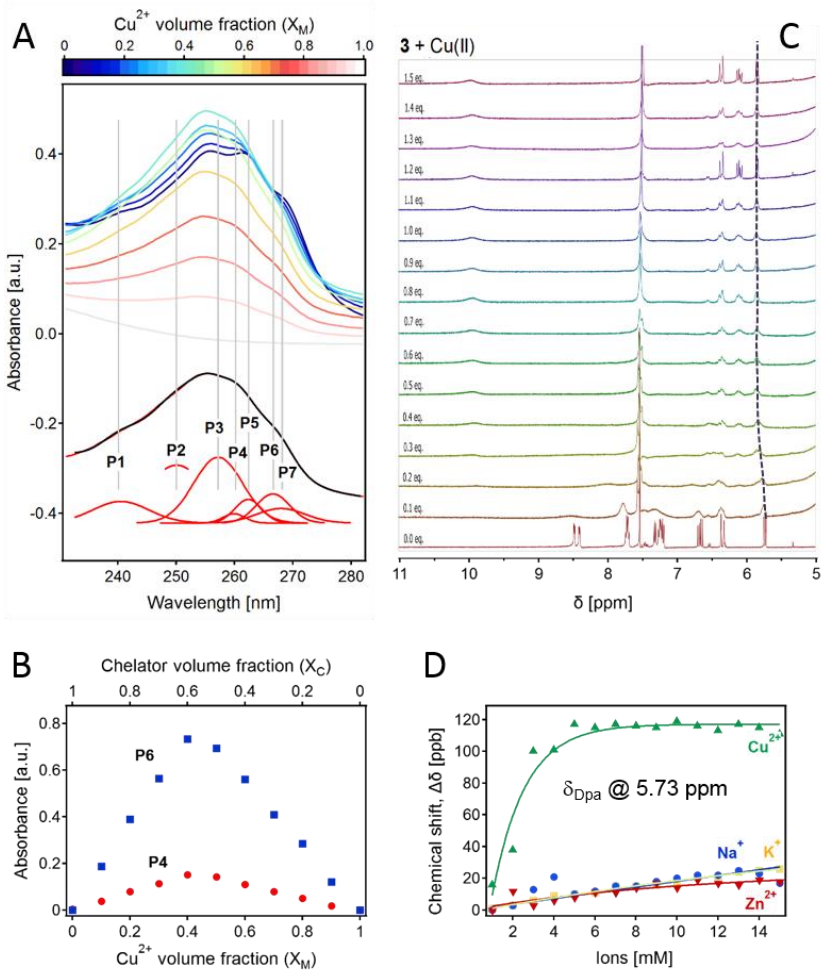

E

Cu^{2+}		Zn^{2+}		Na^{+}		K^{+}	
K_a [M^{-1}]	$\Delta\delta_{max}$ [ppb]	K_a [M^{-1}]	$\Delta\delta_{max}$ [ppb]	K_a [M^{-1}]	$\Delta\delta_{max}$ [ppb]	K_a [M^{-1}]	$\Delta\delta_{max}$ [ppb]
3389	110	409	14	808	18	538	17

Fig. 3: Chelating properties of Cu^{2+} and Dpa-lipid probes. **(A)** Absorption spectra of solutions containing varying ratios of Cu^{2+} and Dpa-lipid (compound **3**) in acetonitrile (Table S1) and an example of fit. **(B)** Job's plot of **3.Cu²⁺** related peaks at 260 nm and 266.5 nm. **(C)** NMR measurements of **3.ion** complexation and **(D)** chemical shift $\Delta\delta$ of Dpa peak at 5.73 ppm versus ions (Cu^{2+}, Zn^{2+}, K^{+}, Na^{+}) concentrations. **(E)** Affinity constants and maximum chemical shift extracted from NMR data using the Rose-Drago method.

spectroscopies association constants, K_a, of **3.X^{n+}** could be determined using the Benesi-Hildebrand (Benesi, 1949) and Rose-Drago methods (S5), respectively (Fig. 3C, 3E) (Rose and Drago, 1959; Wachter and Fried, 1974; Fielding, 2000) for Cu^{2+} and potential competitive ions. Di-picolylamine (Dpa) is a well-known chelator of Cu^{2+} ions and was already tested in several other studies for a whole range of ions (Hoorn et al., 1996; Cho et al., 2019; Dugandžić et al., 2019). These studies evidenced that putative competitive ions such as Zn^{2+}, Ni^{2+}, Co^{2+}, Cd^{2+}, Fe^{2+}, Ca^{2+}, Mg^{2+} have similar affinities (or complexation capacities) for Dpa, which are however much smaller than Cu^{2+}. Therefore, in our study

we have selected Zn^{2+} as one of the competitors to Cu^{2+}. Besides, we have also tested Na^{+} and K^{+} which are the two most common ions in biological fluids.

NMR measurements were conducted as follows: compound **3** was dissolved in a 1:1(V:V) mixture of deuterated chloroform and methanol while cations were dissolved-in water. Affinity constants were extracted using the chemical shift of Dpa chelator peak at 5.73 ppm (Fig. 3D). An affinity constant of ~$3.3.10^3$ M^{-1} was obtained for **3.Cu^{2+}** complex and in the range 4-8.10^2 M^{-1} for the other complexes highlighting a higher selectivity toward Cu^{2+}. De novo, on the basis of these experiments, it is unequivocally confirmed that the highest observed effect is achieved for Cu^{2+} even in a competitive polar medium.

3.3. Sensitivity of the sensor

The sensitivity of the sensor was first tested for specific recognition of copper (II) ions using a range of solutions of copper sulfate solutions at concentrations varying from 1 aM to 10 mM. The sensor response was extracted from successive transfer curve measurements at the different concentrations for V_{TG} in the range -1 V to 2 V while V_{DS} and V_{BG} are kept at respective constant potential values of -2 V and -17 V. Typical transfer curves are shown in Fig. 4A, with the red dotted curve being the reference obtained from DI-water. As expected for a *p*-type MOSFET working in depletion mode, a linear decrease of the I_{DS} values was obtained as the concentration of copper cations was gradually increased in the solution, therefore showing a good response of the sensor. The sensor sensitivity can then be expressed either from the change of the current I_{DS} at a given V_{TG} or from the change of V_{TG} for a given value of I_{DS} in the linear region of the transfer curve as indicated by the dotted black lines. For the later δV_{TG} corresponds to the change in threshold voltage. It is important to notice that at V_{TG}=0 V, the changes in I_{DS} for the different concentrations correspond to the change in the on-state current, I_{DS}(ON). For both cases two examples are shown in Fig. 4B at constant values of V_{TG} of -0.5 V (green) and of I_{DS} of 0.4 μA (blue) respectively. Remarkably, the resulting curves are nearly perfectly superimposed highlighting the fact that both ways are suitable. The red markers on both curves correspond to the values of I_{DS} and V_{TG} obtained for the DI water reference curve. For Cu^{2+} concentrations from 1 aM to 10 fM, the measurements show no changes of I_{DS} and V_{TG} and the values are very similar to those obtained for DI-water. From 10 fM to 0.1 mM, the changes in I_{DS} and V_{GS} decrease linearly with the logarithm of the concentration. Above 0.1 mM, the curves show sublinear behavior indicating that saturation of the sensor is reached. From these data one can clearly conclude that our sensor exhibits a limit of

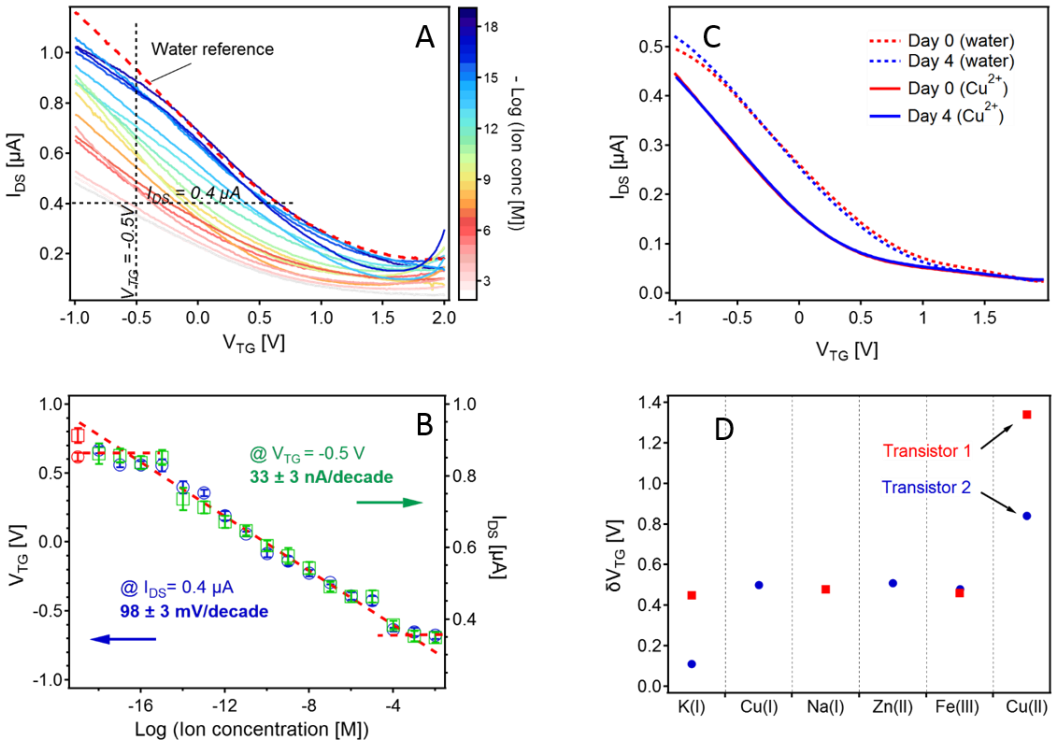

Fig. 4. (A) Transfer curves obtained after exposing the sensor to different concentrations of Cu^{2+} in water ranging from 10 mM to 1 aM. **(B)** Sensor response was extracted from the transfer curves by measuring either the change in current I_{DS} at V_{TG}=-0.5V in the (quasi-) linear region of the curves (green) or the change in V_{TG} at I_{DS}=0.4 µA (blue) versus the logarithm of ion concentration. The red points correspond to the reference measurements. **(C)** Stability of the sensor and reproducibility of the measurement after a succession of 92 measurements spread over a 4 days' time frame. The two sets of data were obtained at a concentration of 12 pM **(D)** Selectivity measurements obtained using two different transistors: Variation of V_{TG} after exposing the sensor to solutions containing K^+, Cu^+, Na^+, Zn^{2+} and Fe^{3+} and Cu^{2+} ions, at a concentration of 1 mM in water.

detection of 10 fM and provides linear quantification of the detection over 10 decades in the range 10 fM to 0.1 mM. Importantly, such low limit of detection is three order of magnitude lower than for ICP-MS (Kilic et al., 2018; Quinn et al., 2018), the most sensitive method so far.

Linear fitting of the I_{DS} curve leads to a current of 33 ± 3 nA/decade. This value represents the sensitivity in drain-source current of the device and appears relatively low. However, the sensitivity could be dramatically improved by optimizing the design of the sensor for instance by changing the channel geometry; increasing the width/length ratio (W/L) would certainly improve the sensitivity in current (in our case W/L=1). In contrast, the linear fitting of the V_{TG} curve leads to a sensitivity of 98 ± 3 mV/decade which surpasses by a factor of three the Nernst limit of 29.5 mV/decade expected for a divalent ion (Chen et al., 2011; Knofmacher et al., 2012). This result is quite surprising considering that in our previous work on Fe^{3+} sensing (Nguyen 2013, 2014), for which the transistor was only gated by the top-gate, the sensor response was Nernstian. We therefore attribute this behavior to the fact that in the present case the sensor is dual-gated. Such super-Nernstian

behavior has been assigned to the coupling between the two top-gate and back-gate capacitances as already demonstrated for dual-gated ISFET pH sensors (DG-ISFET) by several reports in the literature (Knofmacher et al., 2012; Spijkman et al., 2010, 2011; Jang and Cho, 2014; Wu et al., 2017; Spanu et al., 2017). However, to the best of our knowledge this is the first time that such behavior is reported for a metal ion FET sensor. In addition, such behavior has always been reported for DG-ISFET working in enhancement mode using two inorganics dielectrics but never in depletion mode or using a hybrid coupling between inorganic and organic dielectrics.

A major issue of FET sensors used for the detection in solution is the trapping of ions in the dielectric layer, or at its interface with the semiconducting channel, hence creating a surface charge that will screen the charges of the ions we aimed at detecting. The sensor hence loses its sensitivity as the charge builds up. The stability of our sensor over successive measurements was verified over a time frame of 4 days. The two sets of data presented in Fig. 4C were obtained at a concentration of 1 pM using the same sensor in all the experiments presented in this paper (sensor 1). That means that from the first measurement at time=0 and the last measurement at time= 4 days, a set of 92 measurements were performed with different concentrations of Cu^{2+} and other ions. The result shows high reproducibility and stability, and demonstrates that the ion removal protocol described in the *Sensing experiment protocol* section is highly efficient and provides a full recovery of the sensor. The extremely low limit of detection reported here was recently reached for Cu^{2+} using a Si-Nanoribbon ISFET and a Gly–Gly–His peptide as probe (Synhaivska et al., 2019); however, our sensitivity and range of measurements exceed by far all previously reported data.

3.4 Selectivity of the sensor

The selectivity of the device towards Cu^{2+} was explored by exposing the sensor to putative competitive ions (K^+, Cu^+, Na^+, Fe^{3+} and Zn^{2+}) at a concentration of 10^{-3} M. The sensing measurements were conducted under the same conditions as described in the materials and method sections. In this case, the data were extracted from transfer curves obtained from two different transistors with different channel dimensions and working parameters (See S8). Transistor 1 was the same as was used for the sensitivity measurements. Transistor 2 had a channel width and length of 400 μm and 100 μm respectively and was operated with a back-gate biased at -15 V. Exposure to each type of ions leads to a positive sensor response evidenced by a decrease of I_{DS} with respect to the water reference. The

shift δV_{TG}, due to ion complexation with the chelator is reported in Fig. 4D for an I_{DS} value of 0.5 µA. For every tested ion, δV_{TG} is at least two-fold smaller than for Cu^{2+}. These results hence indicate that the sensor although not fully selective, presents higher affinity for Cu^{2+}, in good agreement with the results obtained in solution by NMR. A good level of speciation between Cu^{2+} and Cu^{+} is also noticeable. This is important as the toxicity of dissolved metals is not only related to their concentrations but also to their level of oxidation. Selectivity could be improved by the design and synthesis of new chelator. However, one has to keep in mind that selectivity and reversibility of the complexation, i.e. reinitialization of the sensor, is a stretch; very high selectivity, induced by a high affinity between the chelator and the ion, usually leads to non-reversible processes in a reasonable time scale frame.

4. Conclusions

The first dual-gate ion-FET sensor with an ultra-thin lipid monolayer as top-gate dielectrics was fabricated. The lipid layer was engineered to provide high dielectric performances. The sensor was developed for the detection of Cu^{2+} in solution and the selectivity was obtained by grafting a chelator specific to copper (di-picolylamine derivative) to the lipids head-groups. We report herein unprecedented sensor response with a limit of detection down to 10 fM, a linear dependence over 10 decades, up to 1 mM and a super-Nernstian amplification with a sensitivity of 98 mV/decade of concentration. Super-Nernstian response was previously reported for pH sensor but it is the first time to be reported for an ion sensor. We also showed that the ability of the lipid layer at preventing ions trapping provides a high stability of the sensor over successive measurements. These results are highly promising and will certainly pave the way to new solutions for the detection of small ions at very low concentration.

Acknowledgments

We would like to thank the PLANETE CT-PACA facilities for the use of their nano/micro fabrication platform; Maya Belghazi from the Institute for Neurophysiopathology at Timone Hospital, Marseille, France, for the mass spectroscopy measurements. The project was financially supported by the Agence Nationale de la Recherche (ANR) and the Japan science and technology agency (JST), project No. ANR-16-JTIC-0003-01.

Supporting information

Supporting information file contains: (S1) Chelator synthesis; (S2) Mass spectroscopy of compound ***3***; (S3) 1H-Nuclear Magnetic Resonance spectrum of ***3***; (S4) Job's plot; (S5) Association constant; (S6) Transistor fabrication; (S7) Sensor selectivity transfer curves. The Supporting Information is available free of charge on the ACS Publications website.

References

Arbadi M., Golshani N., 2016. Int. J. Epidemiol. Res. 3, 283-293.

Bhattacharya, S; Snehalatha, K.; Kumar, V. P., J. Org. Chem., 2003, 68, 2741-2747.

Benesi, H. A.; Hildebrand, J. H. J. J. Am. Chem. Soc. 1949, 71, 2703–2707.

Brezoczki V. M., Filip G. M., 2017. IOP Conf. Ser.: Mater. Sci. Eng. 200, 012025.

Charrier A. and Thibaudau F., 2005. Biophys. J. 89, 1094.

Charrier A., Mischki T., Lopinski G.P., 2010. Langmuir 26, 2538.

Chen S., Bomer J.G., Carlen E.T., van den Berg A., 2011. Nano Lett. 11, 2334–2341.

Cho S. W., Rao A. S., Bhunia S., Reo Y. J., Singha S., Ahn K.H., 2019. Sensors & Actuators: B. Chemical 279, 204–212.

Cinti S., Mazzaracchio V., Orturk G., Moscone D., Arduini F., 2018. Anal. Chim. Acta 1029, 1-7.

Das S.K. and Ray K., 2006. Nat. Clin. Pract. Neurol. 2, 482–493.Fielding L., 2000. Tetrahedron 56, 6151-6170.

Dugandžić V., Kupfer S., Jahn M., Henkel T., Weber K., Cialla-Maya D.,Poppet J., 2019. Sensors & Actuators: B. Chemical 279, 230–237.

Dumas C., El Zein R., Dallaporta H., Charrier A.M., 2011. Langmuir *27*, 13643.

El Zein R., Dallaporta H., Charrier A.M., 2012. J. Phys. Chem. *B 116,* 7190.

Fielding L, 2000. Tetrahedron 56, 6151-6170.

Filetti F.M., Vassallo D.V., Fioresi M., Simoes M.R., 2018. Toxicol. in vitro 51, 106-113.

Gao Q., Ji L., Wang Q., Yin K., Lic J., Chen L., 2017. Anal. Methods 9, 5094.

Ghisi M., Chaves E.S., Quadros D.P.C., Marques E.P., Curtius A.J., Marques A.L.B., 2011. Microchem. J. 98, 62–65.

Hoorn H. J., de Joode P., Driessen W. L., Reedijk J., 1996. Recl. Trav. Chim. Pays-Bas 115, 191-197.

Jang H–J. and Cho W.–J., 2014. Sci. Rep. 4, 5284.

Kenaan A., Nguyen T.D., Dallaporta H., Raimundo J.–M., Charrier, A.M., 2016. Anal. Chem. 88, 3804–3809.

Kenaan A., El Zein R., Kilinc V., Lamant S., Raimundo J.-M., Charrier A.M., 2018. Adv. Funct. Mater. 1801024.

Kilic S., Cengiz M.F., Kilic M., 2018. Environ. Monit. Assess. 190, 202.

Knopfmacher O., Tarasov A., Fu W., Wipf M., Niesen B., Calame M., Schönenberger C., 2012. Nano Lett. 10, 2268–2274.

Kubala-Kukuś A., Banaś D., Braziewicz J., Majewska U., Pajek M., Wudarczyk-Moćko J., Antczak G., Borkowska B., Góźdź S., Smok-Kalwat J., 2014. Biol. Trace Elem. Res. 158, 22–28.

Leong W.L., Vittal J.J., 2011. Chem. Rev. 111, 688–764.

Liu Y., Zhu T., Deng M., Tang X., Han S., Liu A., Bai Y., Qu D., Huang X., Qi F., 2018. J. Lumin. 201, 182–188.

Ma S., Lee Y. -K., Zhang A., Li X., 2018. Sens. Actuators B 264, 344-352.

Nguyen T.T.K., Tran H.V., Reisberg S., Noel V., Mattana G., Pham M.C. and Piro M., 2019. Biosens. Bioelectron. 127, 118-125.

Nguyen T.D., El Zein R., Raimundo J.-M., Dallaporta H., Charrier A.M., 2013. J. Mater. Chem. B. 1, 443-446.

Nguyen T.D., Labed A., El Zein R., Lavandier S., Bedu F., Ozerov I., Dallaporta H., Raimundo J.-M., Charrier A.M., 2014. Biosens. Bioelectron. 54, 571-577.

Pimentel L.C.F., de Souza A.L.F., Fernández T.L., Wardell J.L., Antunes O.A.C., 2007. Tetrahedron Lett. 48, 831–833.

Quinn C.W., Cate D.M., Miller-Lionberg D.D., Reilly T., Volckens J., Henry C.S., 2018. Environ. Sci. Technol. 52, 3567–3573.

Roberts E.A., Schilsky M.L., 2008 Hepatology 47, 2089–2111.

Rose N.J.and Drago R.S., 1959. J. Am. Chem. Soc., 81, 6138-6141.

Routasalo T., Helaja J., Kavakka J., Koskinen A.M.P., 2008. Eur. J. Org. Chem. 18, 3190–3199.

Sasaki Y., Minami T., Minamiki T., Tokito S., 2017 Electrochemistry 85, 775–778.

Spanu A., Viola F., Lai S., Cosseddu P., Ricci P.C., Bonfiglio A., 2017. Org. Electron. 48, 188-193.

Spijkman M.-J., Brondijk J.J., Geuns T.C.T., Smits E.C.P., Cramer T., Zerbetto F., Stoliar P., Biscarini F., Blom P.W.M., de Leeuw D.M., 2010. Adv. Funct. Mater. 20, 898–905.

Spijkman M., Smits E.C.P., Cillessen J.F.M., Biscarini F., Blom P.W.M., de Leeuw D.M., 2011. Appl. Phys. Lett. 98, 043502.

Strungaru S.A., Nicoara N., Teodosiu C., Baltag E., Ciobanu C., Plavan G., 2018. Chemosphere 207, 192-202.

Sumby C.J., 2011. Coord. Chem. Rev. 255, 1937–1967.

Swavey S. and Brewer, K. Comprehensive Coordination Chemistry II, Oxford, USA, 2004.

Synhaivska O., Mermoud Y., Baghernejad M., Alshanski I., Hurevich M., Yitzchaik S., Wipf M., Calame M., 2019. Sensors 19, 4022

Takagiri T., Ikuta T., Maehashi K., 2020. ACS Omega 5, 877–881.

Wachter H.N. and Fried V., 1974. J. Chem Edu. 51, 798-799.

Wang T., He T., Yun J. –H., Hu Y., Xiao M., Du A., Wang L., 2018. Adv. Funct. Mater. 28, 1802685.

Wolowicz A. and Hubicki Z., 2012. Chem. Eng. J. 197, 493-508.

Wong Y.-L., Mak C.-Y., Kwan H.S., Lee H.K., 2010. Inorg. Chim. Acta. 363, 1246–1253.

Wu T., Alharbi A., You K.–D., Kisslinger K., Stach E.A., Shahrjerdi D., 2017. ACS Nano 11, 7142–7147.

Wustoni S., Hideshima S., Kuroiwa S., Nakanishi T., Mori Y., Osaka T., 2015. Analyst 140, 6485–6488.

Zhang J., Wua J., Tang G., Feng J., Luo F., Xu B., Zhang, C., 2018. Sens.Actuators, B. Chemical 272, 166–174.

GRAPHICAL ABSTRACT